

# Surface Rupturing Earthquakes of the Greater Caucasus Frontal Thrusts, Azerbaijan

Ian Pierce<sup>1</sup>, Ibrahim Guliyev<sup>2</sup>, Gurban Jalal Yetirmishli<sup>3</sup>, Rauf Muradov<sup>3</sup>, Sabina Kazimova<sup>3</sup>, Rashid Javanshir<sup>4</sup>, Ben Johnson<sup>1</sup>, Neill Marshall<sup>1</sup>, Richard Thomas Walker<sup>1</sup>, and Paul Wordsworth<sup>1</sup>

<sup>1</sup>University of Oxford

<sup>2</sup>Azerbaijan National Academy of Science

<sup>3</sup>Republican Seismic Survey Center of Azerbaijan National Academy of Science

<sup>4</sup>Azerbaijan National Academy of Sciences

December 20, 2022

## Abstract

Quaternary convergence at rates of  $\sim 10$  mm/yr between the Arabian and Eurasian plates is largely accommodated by the Kura fold-thrust belt at the longitude of the Greater Caucasus Mountains in Azerbaijan and eastern Georgia. Here we present the results of the first paleoseismic study of the Kura fold-thrust belt in Azerbaijan. A single paleoseismic trench was excavated across a 2-m-high fault scarp near Agsu revealing evidence of two recent surface rupturing earthquakes. Radiocarbon dating of the faulted sediments places limits of earthquake timing of AD 1713-1895 and AD 1872-2003 for the two events. Allowing for uncertainties in radiocarbon dating, the two events likely correspond to historical destructive  $M \sim 7$  earthquakes near Shamakhi, Azerbaijan in AD 1668 and 1902. Holocene shortening and dip-slip rates for the Kura fold-thrust belt are 8 and 8.5 mm/yr, respectively, based on the depositional age of an abandoned uplifted strath terrace in a water gap to the west of Agsu. These rates should be treated as maxima, as they are  $\sim 100\%$  of the previously determined structurally and geodetically measured shortening across the belt, and were measured from only one of two primary structures in this part of the belt. The lack of reported historical ruptures from the past 8 centuries to the west of Agsu, in contrast with the numerous recorded destructive earthquakes of the Shamakhi region, suggests that the central and western parts of the Kura fold-thrust belt produce less frequent, but more destructive earthquakes, and may have accumulated sufficient strain to produce a  $M > 8$  earthquake.

## Hosted file

952184\_0\_art\_file\_10536772\_rmwhh9.docx available at <https://authorea.com/users/524607/articles/613996-surface-rupturing-earthquakes-of-the-greater-caucasus-frontal-thrusts-azerbaijan>

1  
2 **Surface Rupturing Earthquakes of the Greater Caucasus Frontal Thrusts,**  
3 **Azerbaijan**

4 **Ian Pierce<sup>1</sup>**

5 **Ibrahim Guliyev<sup>2</sup>**

6 **Gurban Yetirmishli<sup>3</sup>**

7 **Rauf Muradov<sup>3</sup>**

8 **Sabina Kazimova<sup>3</sup>**

9 **Rashid Javanshir<sup>1,2</sup>**

10 **Ben Johnson<sup>1</sup>**

11 **Neill Marshall<sup>1</sup>**

12 **Richard Walker<sup>1</sup>**

13 **Paul Wordsworth<sup>1</sup>**

14  
15 <sup>1</sup> University of Oxford, 3 S Parks Road, Oxford, United Kingdom OX13AN

16 <sup>2</sup> Azerbaijan National Academy of Science, Baku, Azerbaijan

17 <sup>3</sup> Republican Seismic Survey Center of Azerbaijan National Academy of Science, Baku,  
18 Azerbaijan

19  
20 Corresponding author: Ian Pierce ([ian.pierce@earth.ox.ac.uk](mailto:ian.pierce@earth.ox.ac.uk))

21 **Key Points:**

- 22 • A paleoseismic trench near Aghsu, Azerbaijan provides evidence of two surface rupturing  
23 events since medieval times.
- 24 • These events occurred AD 1713-1895 and 1872-2003, and may correspond to historical  
25 earthquakes that destroyed Shamakhi in 1668 and 1902.
- 26 • Maximum shortening and dip-slip rates of the frontal thrust sheet in the eastern Kura  
27 fold-thrust belt are 8 and 8.5 mm/yr, respectively.

28

**29 Abstract**

30 Quaternary convergence at rates of  $\sim 10$  mm/yr between the Arabian and Eurasian plates  
31 is largely accommodated by the Kura fold-thrust belt at the longitude of the Greater Caucasus  
32 Mountains in Azerbaijan and eastern Georgia. Here we present the results of the first  
33 paleoseismic study of the Kura fold-thrust belt in Azerbaijan. A single paleoseismic trench was  
34 excavated across a 2-m-high fault scarp near Aghsu revealing evidence of two recent surface  
35 rupturing earthquakes. Radiocarbon dating of the faulted sediments places limits of earthquake  
36 timing of AD 1713-1895 and AD 1872-2003 for the two events. Allowing for uncertainties in  
37 radiocarbon dating, the two events likely correspond to historical destructive  $M \sim 7$  earthquakes  
38 near Shamakhi, Azerbaijan in AD 1668 and 1902. Holocene shortening and dip-slip rates for the  
39 Kura fold-thrust belt are 8 and 8.5 mm/yr, respectively, based on the depositional age of an  
40 abandoned uplifted strath terrace in a water gap to the west of Aghsu. These rates should be  
41 treated as maxima, as they are  $\sim 100\%$  of the previously determined structurally and geodetically  
42 measured shortening across the belt, and were measured from only one of two primary structures  
43 in this part of the belt. The lack of reported historical ruptures from the past 8 centuries to the  
44 west of Aghsu, in contrast with the numerous recorded destructive earthquakes of the Shamakhi  
45 region, suggests that the central and western parts of the Kura fold-thrust belt produce less  
46 frequent, but more destructive earthquakes, and may have accumulated sufficient strain to  
47 produce a  $M > 8$  earthquake.

48

**49 Plain Language Summary**

50 The Greater Caucasus Mountains stretching between the Black and Caspian Seas are a result of  
51 the northward subduction of the Arabian plate beneath Eurasia. For the last 2 million years, most  
52 of this plate motion has been accommodated by the Kura fold-thrust belt in Azerbaijan & eastern  
53 Georgia. This plate motion produces periodic large earthquakes. Here a paleoseismic trenching  
54 investigation revealed evidence of two large earthquakes in the eastern part of the Kura fold-  
55 thrust belt. These earthquakes likely correspond to known historical earthquakes in 1668 and  
56 1902. A lack of historical earthquakes to the west of this study area suggests that the rest of the  
57 Kura fold-thrust belt may produce less frequent, but more devastating earthquakes along this  
58 plate boundary.

59

60

## 61 1 Introduction

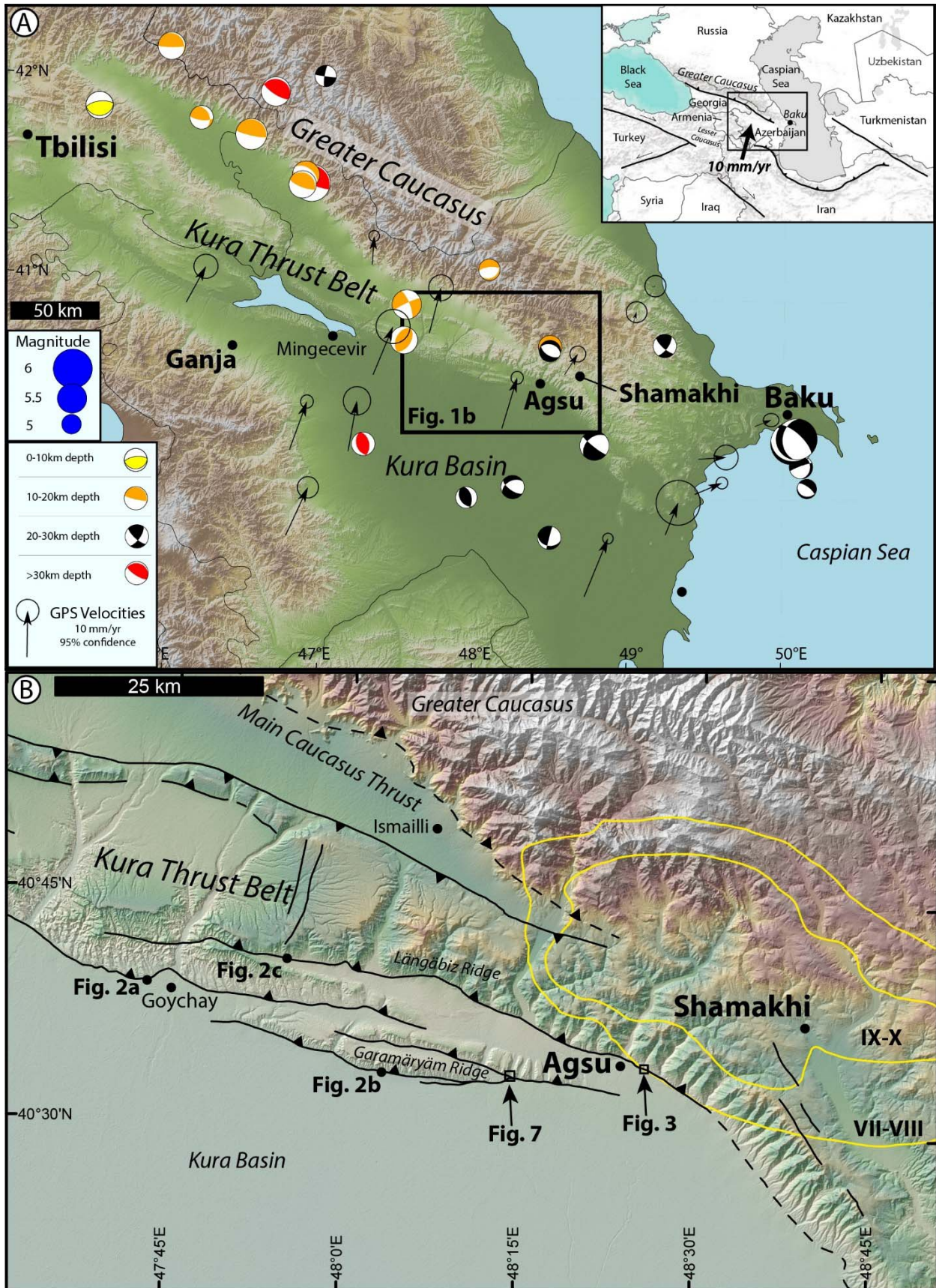
62 The Greater Caucasus Mountains stretch for 900 km between the Black and Caspian Seas  
63 (**Figure 1**). The Greater Caucasus have been uplifted since  $\sim 5$  Ma as a result of the northeast-  
64 directed subduction of the Arabian plate beneath the Eurasian plate (Avdeev and Niemi, 2011;  
65 Cowgill et al., 2016; Forte et al., 2015; Gunnels et al., 2021; Jackson et al., 2002; Kangarli et al.,  
66 2018; McKenzie, 1972; Mumladze et al., 2015; Philip et al., 1989). This subduction has been  
67 largely accommodated by the north-dipping Main Caucasus Thrust Fault, and since  $\sim 1.5$  Ma via  
68 the foreland Kura fold-thrust belt, at an average rate of 6.7-13.6 mm/yr, measured from restored  
69 balanced cross sections (Forte et al., 2013; Kangarli et al., 2018; Mosar et al., 2010), or  $\sim 10$   
70 mm/yr measured by GPS across the Kura basin (Kadirov et al., 2012; Reilinger et al., 2006;  
71 Yetirmishli et al., 2022).

72 The Kura fold-thrust belt extends roughly west-east for  $\sim 275$  km from near Tbilisi,  
73 Georgia to near Shamakhi, Azerbaijan (**Figure 1**). The belt forms an imbricate pattern that varies  
74 along strike with between one and four thrust sheets reaching the surface. Historical destructive  
75 earthquakes in the region are well known from AD 1139, 1668, and 1828-1902 (Ismail-Zadeh et  
76 al., 2020). The 1668 and 1828-1902 events all occurred near Shamakhi (**Figure 1**), in the  
77 easternmost part of the Kura fold-thrust belt. Despite the seismic history of the region, we are  
78 aware of no prior neotectonic or paleoseismic studies that have been conducted on the faults  
79 within the Kura fold-thrust belt, nor anywhere within Azerbaijan, so the source faults of these  
80 historical earthquakes remain unknown. Jackson and Ambraseys (1997) demonstrate that  
81 historical seismicity over the past 400 years accounts for only 25% of shortening in the  
82 Caucasus. This leads to great uncertainty in the seismogenic potential of the faults in this region  
83 as it is unclear whether the lack of historical seismicity to the west of Shamakhi is a result of  
84 either (a) a lapse of historical record keeping, (b) aseismic deformation (e.g. fault creep), or (c)  
85 unreleased moment that is accumulating in the Kura fold-thrust system.

86 Thus, investigating the paleoseismic history of the faults in the Kura fold-thrust belt is  
87 critical for understanding the seismic potential and behavior of the faults in this region. In this  
88 paper we present the results of the first paleoseismic trench investigation and a slip rate estimate  
89 from the Kura fold-thrust belt in Azerbaijan. We then provide a brief discussion on the  
90 significance of these results and place them in the context of the historical catalog.

91  
92 **Figure 1.** (Following page) Overview map of (A) Azerbaijan showing GPS velocities relative to  
93 stable Eurasia (Kadirov, 2012), and focal mechanisms of earthquakes from the gCMT and  
94 gWFM catalogues with ISC-EHB hypocentres from 1976-present. (B) is the eastern part of the  
95 Kura fold-thrust belt showing major faults (black lines, dashed where approximate) and figure  
96 locations. The Kura fold-thrust belt has accommodated  $>80\%$  of the shortening between the  
97 Lesser Caucasus and Greater Caucasus since  $\sim 1.5$  Ma, at an average rate of  $\sim 7$ -14 mm/yr (Forte  
98 et al., 2013). Yellow lines are MMI scale isoseismals of the 1902 Shamakhi earthquake adapted  
99 from Weber (1902). Inset simplifies major regional tectonic faults and representative GPS  
100 velocity relative to stable Eurasia.

101



103

104 **2 Methods**

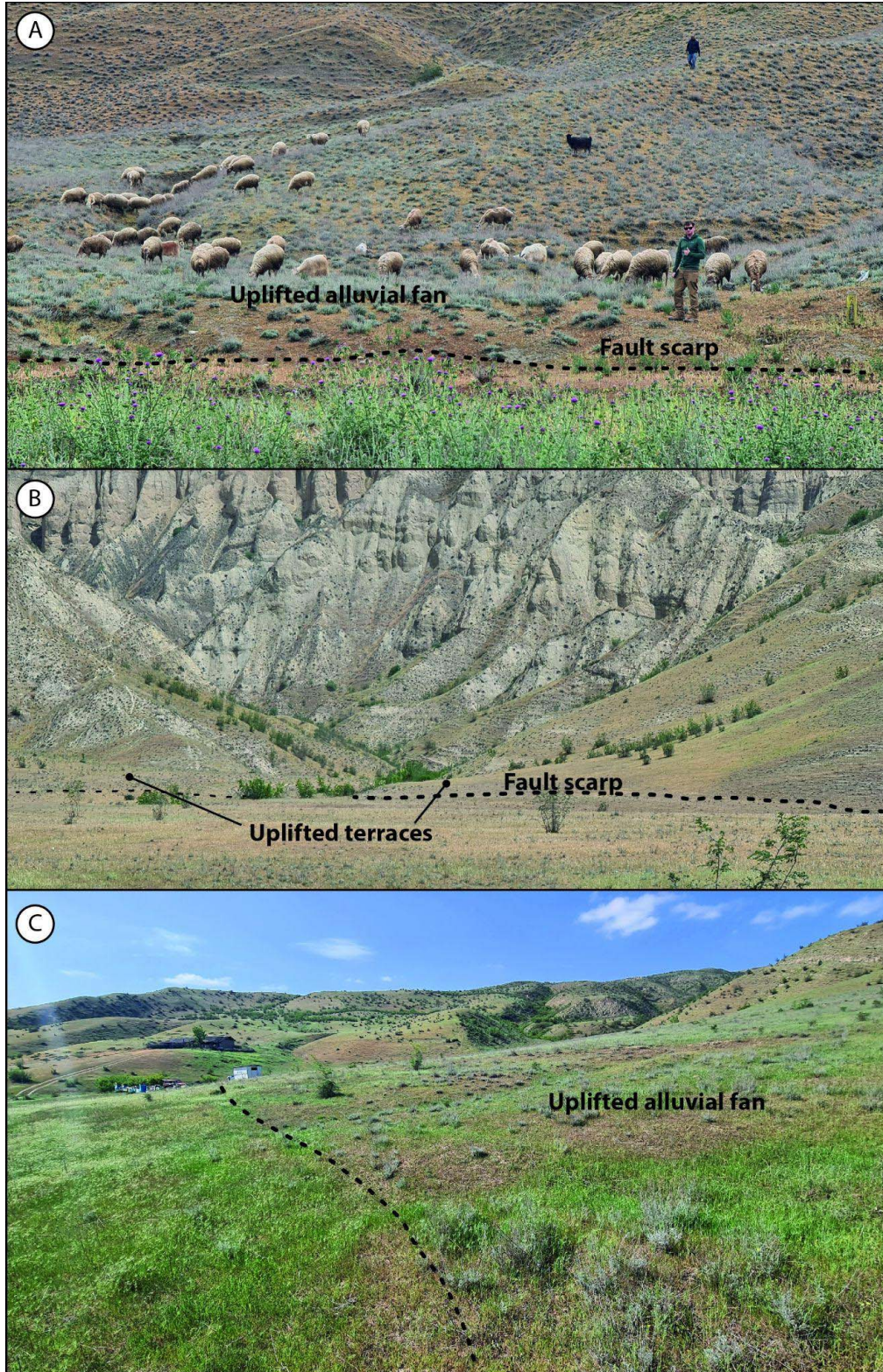
## 105 2.1 Fault Mapping, Photogrammetry, and Paleoseismic Trenching

106 Faults were remotely mapped using Google Earth, prior to field reconnaissance mapping  
107 in the spring of 2022. Key study sites were then surveyed in high detail with photogrammetry  
108 using images captured with a Teokit-equipped DJI Phantom 4 Pro v2 drone. The Teokit is a  
109 dGPS used for acquiring precise photo locations that are then corrected to an Emlid Reach RS2  
110 dGPS base station (e.g., Zhang et al., 2019). The resulting photographs were processed using  
111 Agisoft Metashape software into DEMs and Orthomosaics, with resolutions of 6-10 and 3-5  
112 cm/pixel, respectively (see Data Availability statement for access).

113 A single paleoseismic trench was excavated, cleaned, gridded, and logged. As a base for  
114 logging, an orthophoto mosaic was constructed using Agisoft Metashape software with  
115 photographs captured with a Samsung Galaxy S20 Ultra. The orthophoto was accurately scaled  
116 and oriented using reference points extracted from an iPad-lidar scan of the trench wall (**Pierce  
117 and Koehler, 2022 *in press***). Logging was then conducted on an iPad. Units and faults were  
118 divided and described following standard paleoseismic methods (e.g., McCalpin, 2009),  
119 including sedimentary facies, cross-cutting relations, and development of soils. Radiocarbon  
120 samples of charcoal, plant material, and soil were processed and analyzed at Beta Analytic  
121 laboratory in Miami, Florida, and calibrated using OxCal v4.4 (Bronk Ramsey, 1995) with the  
122 IntCal20 calibration curve. Ages and processing details are listed in **Table 1**.

123

124



125  
126  
127  
128

**Figure 2.** Fault scarps in young geomorphic surfaces show that each of the major thrusts in the Kura fold-thrust belt is active. Locations indicated on Figure 1.

## 129 **3 Results**

### 130 3.1 Fault Mapping

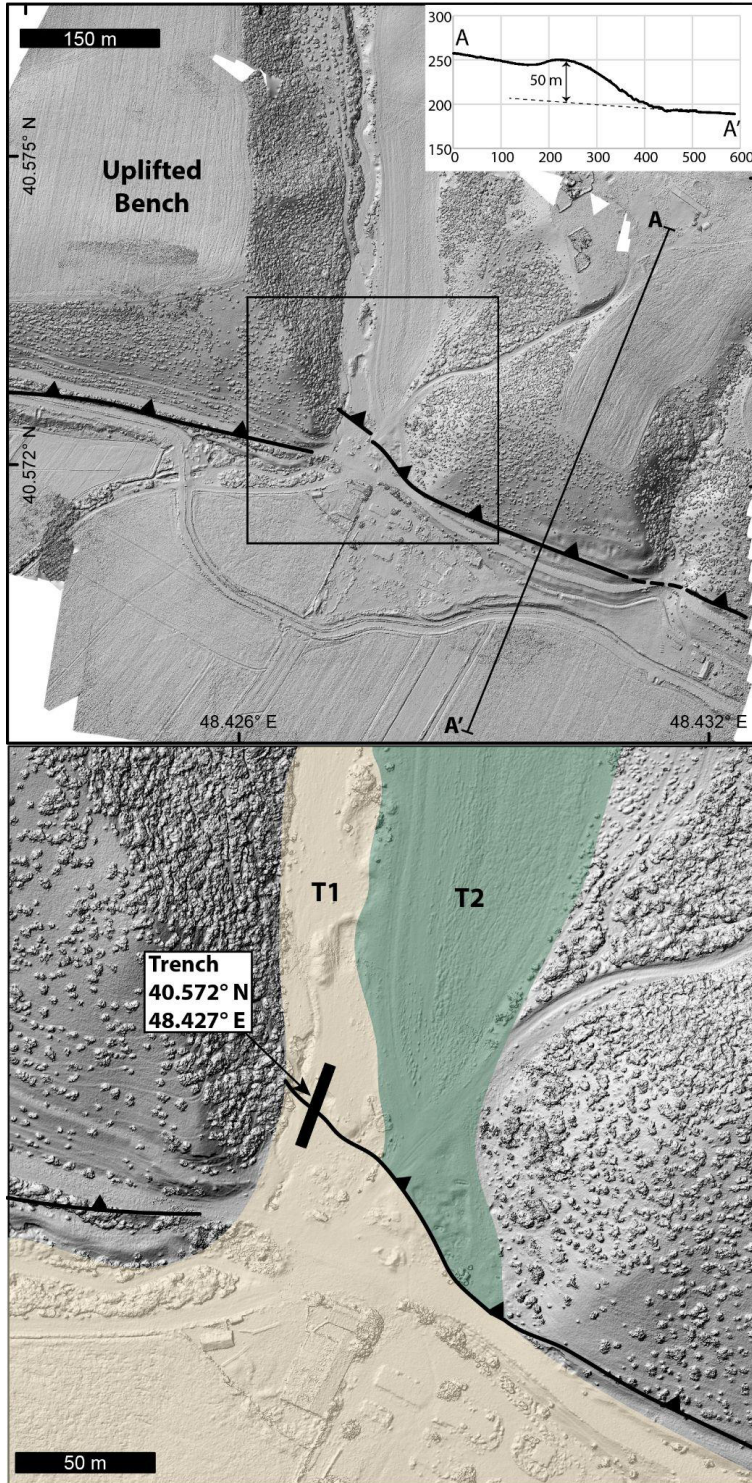
131 Our field reconnaissance focused on the easternmost 60 km of the Kura fold-thrust belt  
132 from near Goychay to Agsu (**Figure 1**). This section of the thrust-belt consists of two major  
133 thrust sheets that each comprise several imbricate thrusts. The more northerly sheet forms the  
134 Längäiz ridge, which is a relay ramp that steps near Goychay. The southerly sheet begins to the  
135 east of Goychay and increases in relief eastward as it forms a large anticline (the Garamäyäm  
136 ridge) before tapering and finally disappearing just south of Agsu. Near the center of the  
137 Garamäyäm ridge the southerly sheet is split into two thrusts, which merge eastward. Field  
138 surveys revealed fault scarps and uplifted youthful geomorphic surfaces on all of these different  
139 fault strands (**Figure 2**), which suggests that each of these thrusts has been active in the  
140 Holocene and periodically ruptures to the ground surface during large earthquakes.

141

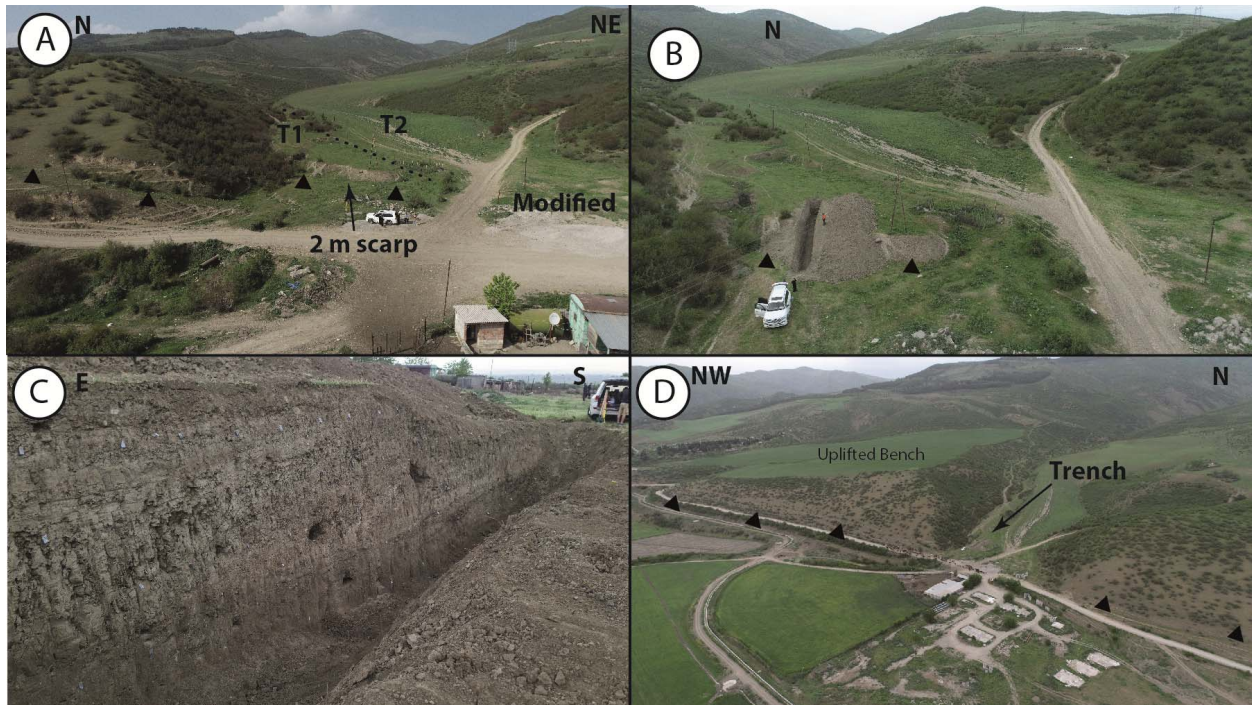
### 142 3.2 Paleoseismic Trenching

#### 143 3.2.1 Description of Trench Site

144 The Kura thrust immediately adjacent to Agsu follows the range front of the Greater  
145 Caucasus. Here the active fault forms a ~50-m-high back-tilted uplifted bench along the  
146 range front, with a clear fold in the crest of the uplifted surface (**Figure 3**). Approximately 2.5 km  
147 east of Agsu is a small alluvial valley where a stream has incised through this bench, cutting  
148 perpendicularly to the fault trace (**Figures 3 and 4**). This valley contains two low incised  
149 terraces, a lower T1 terrace and a 1-m-higher T2 terrace. The two terrace treads are smooth,  
150 relatively flat, and continuously traceable upstream from the valley mouth for ~300 m (**Figure**  
151 **4A**). At the valley mouth, both terraces are displaced, with fault scarps that are ~2 m high. On  
152 the western margin of the valley a small stream has sharply incised into the T1 terrace. The  
153 drone-derived hillshade image shows evidence of anthropogenic modification of the scarp in the  
154 T2 terrace, but both sides of the fault in the T1 terrace appear to be unmodified and correlative.  
155 A paleoseismic trench was excavated across the 2-m-high scarp cutting across the T1 terrace in  
156 this alluvial valley.



157  
 158 **Figure 3.** Hillshade image of photogrammetry-derived DEM of the trench site east of Agsu.  
 159 Inset topographic profile shows characteristic folding of the 50-m-high uplifted bench along the  
 160 rangefront here. Lower panel shows T1 and T2 terraces within the small alluvial valley.

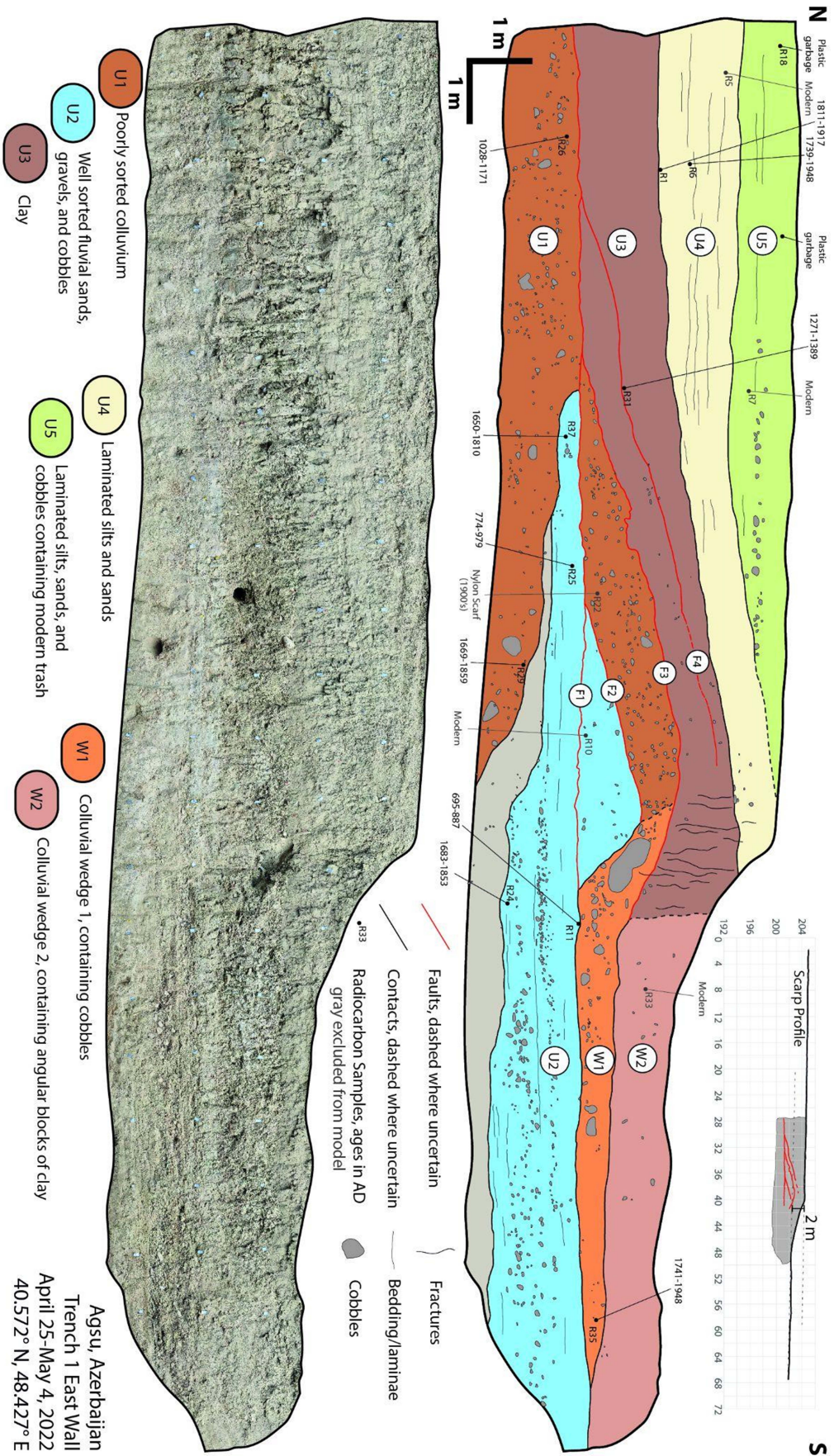


161  
 162 **Figure 4.** Aerial photographs of the trench site before (A) and after (B) trench excavation,  
 163 highlighting the 2-m-high scarp and small alluvial valley. (C) shows the excavated trench. (D)  
 164 shows the uplifted folded bench along the range front.  
 165

### 166 3.2.2 Description of Trench Exposure

167 The trench exposure was 22-m-long and 5-m-deep (**Figure 5**). The trench revealed a  
 168 series of clays, alluvium, and colluvium that are cut and deformed by a low angle fault. The  
 169 lowest unit in the trench, U1, is a colluvial deposit that consists of poorly sorted rounded cobbles  
 170 and gravels in a fine grained silty/sandy matrix. Onlapping onto U1 is U2, a south-thickening  
 171 sequence of interbedded, well-sorted, grain-supported fluvial sands, gravels, and rounded  
 172 cobbles. At the top of U2 is a ~40-cm-thick fine grained, light colored paleosol, that is readily  
 173 traced across much of the trench. Above U1 in the hanging wall is U3, a 1.5-m-thick finely  
 174 laminated clay that dries into prismatic blocks, and is highly sheared near the fault zone. Above  
 175 U3 is U4, a sequence of clays, silts and sands with fine laminations. Above U4 is U5, a series of  
 176 laminated silts and sands with a thin layer of cobbles, and scattered modern plastic garbage in the  
 177 upper 20-30 cm. Above U2 is a poorly sorted colluvial unit, W1, composed of rounded cobbles  
 178 and gravels in a fine grained matrix. At the top of W1 is a ~20-cm-thick, light-colored fine-  
 179 grained paleosol. W1 is thickest directly below the fault scarp and tapers away from the scarp to  
 180 the south. Above W1 is W2. W2 is another colluvial unit, composed of angular blocks of clay in  
 181 a fine grained matrix with very few scattered pebbles.

182 A sub-horizontal fault cuts across the trench exposure and splays into 4 sub-faults in the  
 183 hanging wall (faults F1 to F4). Fault F4 forms a shear zone within U3. Faults F3 and F2 bound a  
 184 shear zone composed of materials from U1 and are well marked by alignments of cobbles and  
 185 pebbles. Fault F1 displaces part of the soil capping U2. Units U1, U2, U3, and U4 are clearly  
 186 folded in the hanging wall of the trench, while U2 is largely undeformed in the footwall.  
 187



189 **Figure 5 (previous).** Trench log (upper) and photomosaic (lower) of the east wall of the Agsu  
190 trench. Inset shows position of trench within fault scarp profile. Ages listed are modeled ages as  
191 described in text. We interpret evidence of two events primarily based on the colluvial wedge  
192 stratigraphy on the footwall (W1 and W2).

### 193 3.2.3 Event History

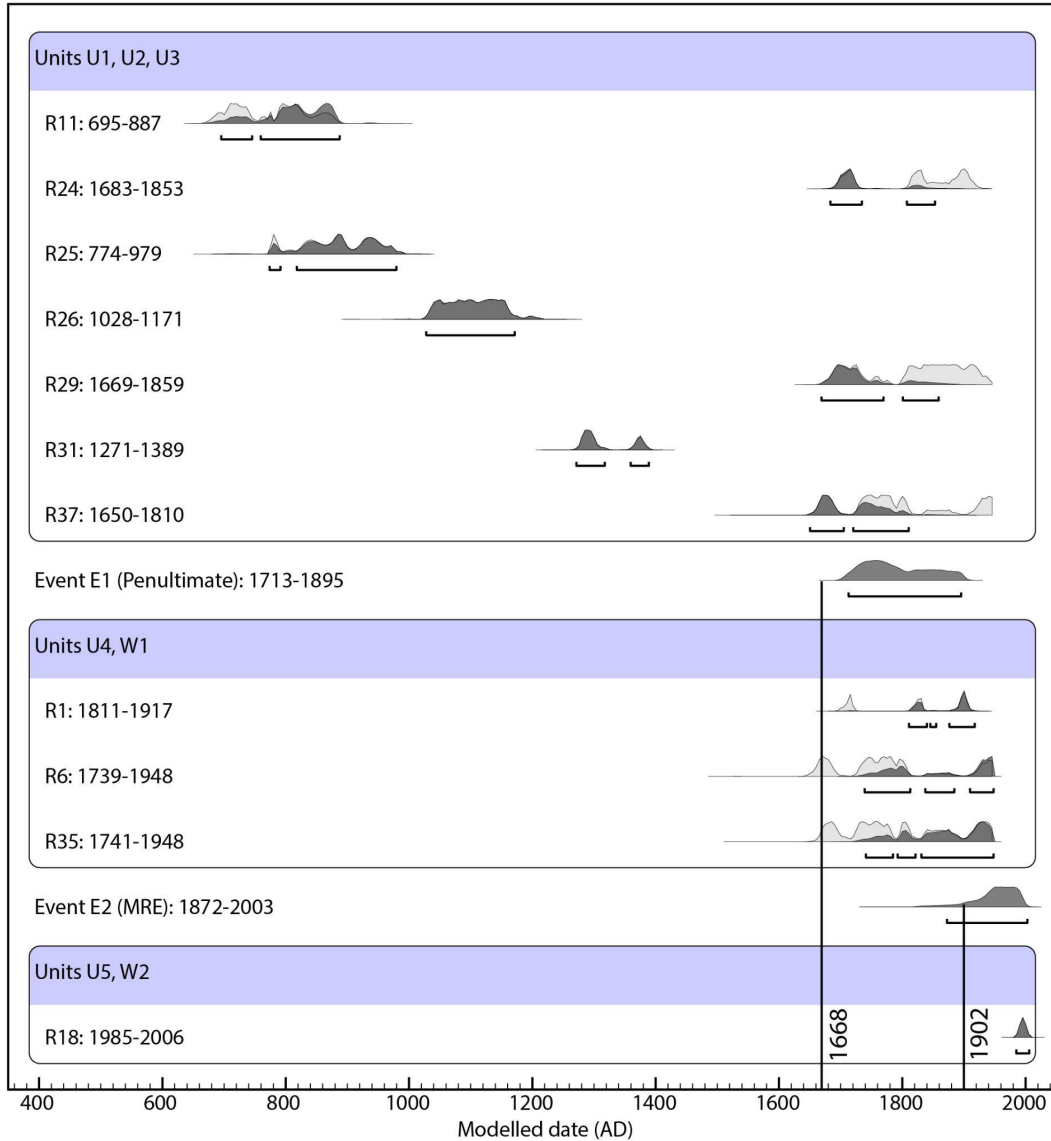
194 The stratigraphy on the southern half of the trench provides evidence of two rupturing  
195 events, clearly demarcated by the two distinct colluvial wedges (W1 & W2) resting upon  
196 undeformed fluvial sediments (U2) (**Figure 5**). The older, penultimate event (E1) produced the  
197 W1 colluvial wedge composed of unsorted gravels and cobbles that bury the paleosol capping  
198 the lower U2 fluvial sediments. This W1 wedge then developed a thin, fine-grained soil on its  
199 top. The younger, most recent event (E2) produced another colluvial wedge (W2), but composed  
200 of angular blocks of clay sourced from U3. This W2 wedge buried the thin soil capping the W1  
201 penultimate wedge.

202 The penultimate E1 event ruptured the F1 and F2 faults through the U1 colluvial deposit  
203 at the bottom of the north-half of the trench along a sub-horizontal fault plane. This created an  
204 abrupt fold in this U1 colluvial deposit, which then collapsed forming the E1 wedge. The clays  
205 and silts of U4 were then deposited on the hanging wall, behind this fold. A minimum of 6.6 m  
206 of displacement can be estimated for E1 by backslipping U1 along faults F1 and F2.

207 The more recent event, E2, ruptured the F3 fault along the base of the U3 clay, folding  
208 units U3 and U4 into a sharp fold-scarp, and again creating a colluvial wedge, W2. U5, like U4,  
209 represents growth strata deposited behind this fold on the hanging wall. A minimum of 3.5 m of  
210 displacement is required to thrust U3 over the crest of the fold in U1. As units U1 and U3 are  
211 both highly sheared in the fault zone, there is high uncertainty in these offset measurements.

### 212 3.2.4 <sup>14</sup>C Geochronology

213 The radiocarbon ages of 14 total samples of charcoal, organic sediments, and plant  
214 fragments recovered from the strata were measured by Beta Analytic laboratories in Miami,  
215 Florida. The sample locations are indicated on **Figure 5**, and the results are listed in **Table 1**.  
216 Four samples: R5, R7, R10, and R33 yielded modern ages. Of these, R7 and R33 are from post-  
217 earthquake deposits, so the modern ages may be representative of their depositional ages, but due  
218 to uncertainty in the calibration of modern radiocarbon we exclude them from our OxCal model.  
219 R5 and R10, from within layers dated to pre-modern by other samples, are both plant materials  
220 so it is likely that we inadvertently sampled modern plant roots, and thus we exclude them from  
221 further analysis. Sample R22, from within the fault zone (Unit U1), is a large fragment of a nylon  
222 scarf. Nylon was invented in the mid 1900's so we think that this material must have been  
223 brought down to this level by a burrowing animal, as other samples from Unit 1 are medieval in  
224 age (R26: 1028-1171, R29: 1669-1859). Sample R18 was a late 1990's vintage plastic candy  
225 wrapper, so is assumed to be from AD 1995 ± 5, and is used as an upper limit of the stratigraphic  
226 model. The remaining ages were placed into a sequence model and calibrated using OxCal v4.4  
227 (Bronk Ramsey, 1995) (**Figure 6**). The result of this model places limits on the timing of the two  
228 surface rupturing events: E1 occurred from AD 1713-1895, and E2 occurred from AD 1872-  
229 2003 (95.4% confidence intervals).



230

231

232 **Figure 6.** OxCal model of radiocarbon samples and event ages. The timing of the 1668 and 1902  
 233 historical earthquakes are plotted for reference. Event horizons for E1 and E2 are AD 1713-1895  
 and AD 1872-2003, respectively.

233

234

### 3.3 Slip Rate Measurement

235

236

237

238

239

240

241

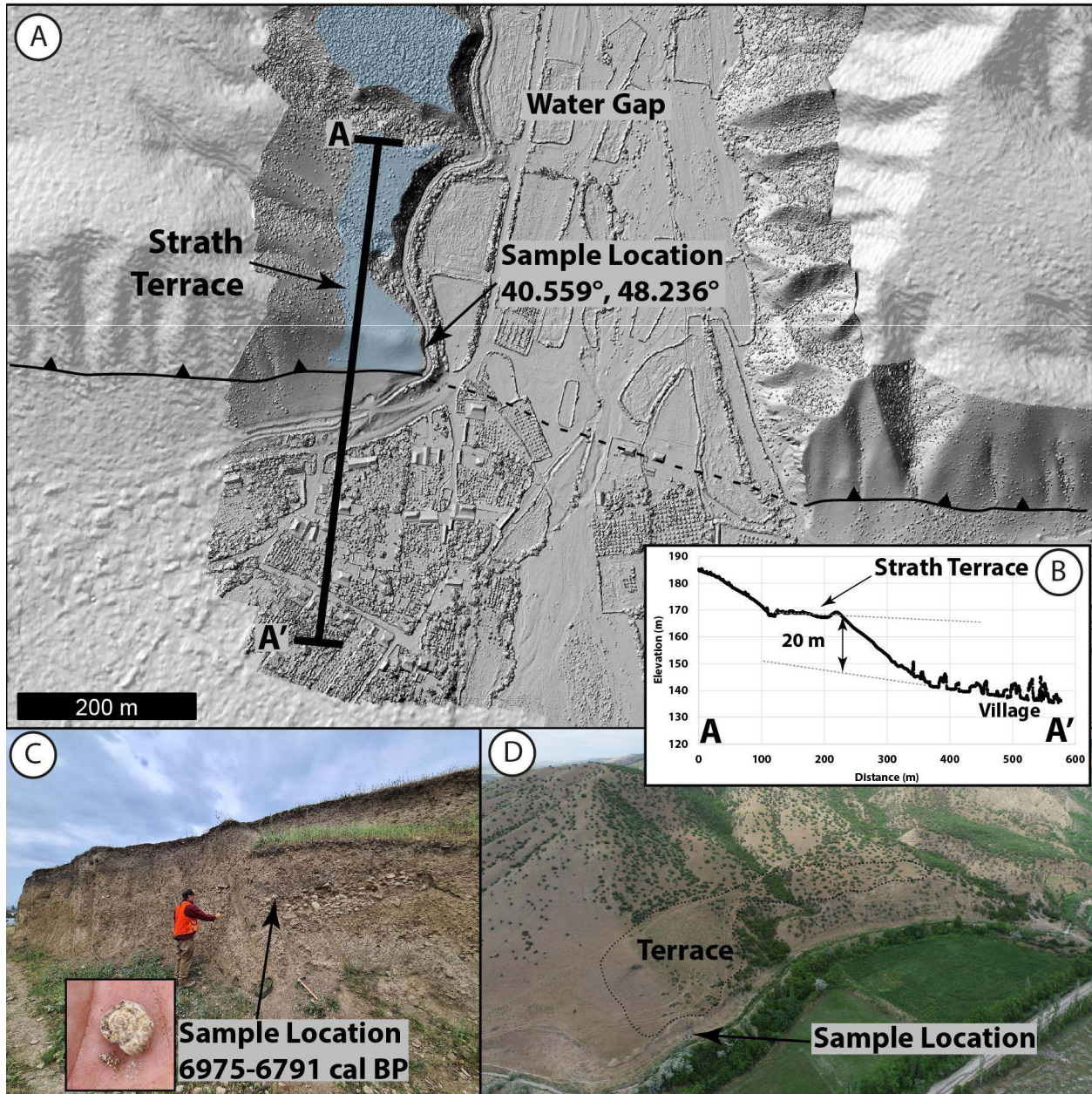
242

243

244

West of Agsu in the foreland is the Garamäyän ridge, a prominent pair of west-northwest-striking active folds are cut by a series of water gaps (Forte et al., 2013). In one of these water gaps (“Gap 2” of Forte et al., 2013) is an inset strath terrace that sits ~20 m above the modern stream. The southern margin of this terrace is abruptly truncated by an active fault and shows a sharp anticline close to the head of the fault scarp. In a cliff exposure cut for an irrigation canal we found a strath of subhorizontal fluvial cobbles capping sub-vertical sand and gravel beds (**Figure 7**). The radiocarbon age dating of a single gastropod shell (WG1, **Table 1**) sampled from within these horizontal sediments allows for calculation of a vertical uplift rate for this fault (Pigati et al., 2010). The OxCal calibrated age of the shell is 6975-6791 cal BP. As shells can contain significant inherited carbon, this should be considered to be the oldest possible

245 age of the deposit. Dividing the 20 m uplift of the terrace (**Figure 7B**) by this age results in an  
 246 average vertical uplift rate of 2.9 mm/yr.  
 247



248 **Figure 7.** Hillshade image of photogrammetry-derived DEM (A) showing the uplifted  
 249 strath terrace inset to the watergap. Profile A-A' shown in (B) shows 20 m of uplift. A gastropod  
 250 shell (inset) was sampled from subhorizontal fluvial cobbles in an exposure of the strath (C).  
 251 Oblique aerial photograph of the terrace (D).  
 252

## 253 4 Discussion

### 254 4.1 Distribution of Slip in the foreland of the Greater Caucasus

255 Converting our 2.9 mm/yr uplift rate at the water gap site (**Figure 7**) to dip-slip and  
256 shortening- rates requires an assumption of subsurface structural geometry. Forte et al. (2013)  
257 model the Garamäyän ridge anticline as a blind fault-propagation fold controlled by a 20°  
258 northeast dipping thrust fault that has accommodated 5.6 km of shortening. Our field  
259 investigations revealed the presence of surficial fault scarps demonstrating that this fault is not  
260 blind. If we assume this 20° dipping thrust fault geometry, and that folding is minimal over the  
261 relatively short ~7 kyr timescale, then 2.9 mm/yr of uplift corresponds to 8.0 mm/yr of  
262 shortening and a dip-slip rate of 8.5 mm/yr. These rates are in-line with the prior structural and  
263 geodetic estimates across the Kura fold-thrust belt (Forte et al., 2013; Kadirov et al., 2012).  
264 Unfortunately, due to the reliance of our calculations on a single age and the uncertainty of the  
265 near-surface fault geometry, the uncertainty of our rates is difficult to quantify. However, as this  
266 rate was determined from only one of the two main active parallel structures at this longitude  
267 (the other was trenched in this study), and this rate consumes nearly all of the budget of the prior  
268 estimates, we expect that this rate is an upper limit. Regardless, this result is consistent with that  
269 of Forte et al. (2013), which demonstrates that a significant portion (~80-100%) of both the post-  
270 1.5 Ma and present-day geodetic strain budget across the Greater Caucasus is accommodated by  
271 the Kura thrust belt.

### 272 4.2 Historical Earthquakes

273 While the Eastern Caucasus have not experienced any  $M > 7$  earthquakes during the  
274 instrumental period (Telesca et al., 2018; Yetirmishli et al., 2021), the region has experienced  
275 numerous pre-instrumental devastating earthquakes, the largest ( $M \sim 7$ ) occurring in AD 1139,  
276 1668, and 1902 (Ismail-Zadeh, 2020). The widely felt 1668 and 1902 earthquakes both destroyed  
277 the medieval capital city of Shamakhi (**Figure 1**), while moderate ( $M \sim 6$ ) events in 1828, 1859,  
278 1869, and 1872 caused severe damage to the city.

279 The 1139 earthquake is reported to have destroyed the city of Ganja in the southwestern  
280 part of the Kura basin (**Figure 1a**). It is unclear whether this event is associated with the Kura  
281 fold-thrust belt, or if it occurred in the Lesser Caucasus. However, the AD 1139 earthquake is the  
282 earliest earthquake record from the Kura region, and as the region has been continuously  
283 inhabited since then, we assume that all significant large earthquakes since that time have been  
284 reported.

285 A fair amount of detail can be gleaned about the 1668 Shamakhi earthquake from  
286 contemporary historical sources (reported dates range from 1667-1669). Some of the most  
287 widely cited accounts of the damage in Western studies come from European travelers passing  
288 through the region around this period. The well-known French traveler, John Tavernier, was in  
289 the region during the earthquake but only heard news of the event while in Tabriz. According to  
290 the account he received the entire city was demolished and only a handful of people survived  
291 (Tavernier, 1678). Somewhat later, Cornelius de Bruijn (translated into English as “Cornelius le  
292 Brun”) visited Shamakhi, and mentioned that the earthquake, which occurred thirty-five years  
293 before his travels in 1703, destroyed all of the city walls and major monuments including the  
294 congregational mosque (Le Brun, 1759). It would appear, however, that the administrative

295 function of the city remained and he mentions smaller mosques and houses that he saw when  
 296 visiting. The impact on the people was severe enough that a tremor during his visit (1703) saw  
 297 people flee the city but there was limited or no damage to structures. It is worth noting that de  
 298 Bruijn's dating places this event in 1668, a date accepted by Nikonov in his comprehensive  
 299 review of the source materials for this earthquake, more specifically he estimates, on the 14<sup>th</sup>  
 300 January (Nikonov, 1982). In his chronological table of events, he notes a number of aftershocks  
 301 ranging from later in 1668, until early 1671. Specific impacts listed by Nikonov based on his  
 302 assessment of all sources available to him include: destruction of the entire city, between 6,000-  
 303 8,000 deceased, large numbers of collapsed individual buildings including the city walls and  
 304 fortress, and landslides causing loss of life (Nikonov, 1982). Sources collated in this work  
 305 detailing other settlements in the region mention impacts as far away as Baku (a collapsed wall  
 306 of a palace), detection but no damage in Derbent, and the event was apparently not felt in the  
 307 more distant heavily-populated regions of Tbilisi or Yerevan. Based on the collective data,  
 308 Nikonov assesses the area of highest impact of the earthquake as IX on the MSK-64 intensity  
 309 scale in the region of Shamakhi.

310 The 1828 event destroyed 526 buildings across the region. The 1859 event killed 100  
 311 people, and destroyed 741 buildings, prompting the capital to be relocated from Shamakhi to  
 312 Baku. The 1872 event killed 118 people and destroyed all but 20 buildings (Shebalin et al.,  
 313 1982). The 1902 event killed 2,000 people and destroyed 4,000 homes (New York Times, 1902).  
 314 An isoseismal plot of damaged buildings from the 1902 earthquake (adapted from Weber, 1903  
 315 in **Figure 1**) suggests that the epicenter was close to Shamakhi and that the fault that ruptured  
 316 follows the overall strike of the Kura thrust.

317 Our paleoseismic results provide evidence of two surface rupturing events since the early  
 318 18th century (E1: AD 1713-1895 and E2: AD 1872-2003). The younger of these rupturing  
 319 events, E2, may be the surface rupture of the 1902 Shamakhi earthquake, while the penultimate  
 320 E1 event could be the 1668 earthquake if we reject two radiocarbon ages (R24 and R29).  
 321 Present-day Shamakhi is only ~18 km northeast of the Agsu trench site, and would have  
 322 experienced high intensity ground motions if the northeast-dipping fault ruptured, so the  
 323 destruction reported during these events is consistent with our paleoseismic results.

324 The past magnitude estimate of  $M \sim 7$  for the 1902 E2 event is reasonable based on  
 325 comparisons of the 3.5 m displacement in the trench to displacements of other surface rupturing  
 326 reverse mechanism earthquakes (e.g. [Wesnousky, 2008](#)), though such comparisons are of limited  
 327 utility due to the paucity of examples of thrust/reverse surface rupturing earthquakes. Based on  
 328 the greater observed displacement, E1 may have had a larger magnitude than E2. If we assume  
 329 that the 1902 rupture plane (E2) has dimensions similar to the reported high damage isoseismals  
 330 (50 x 30 km, Weber, 1903) and slipped an average of 3.5 m (measured from the trench), then  
 331 using the equation relating moment magnitude to seismogenic moment, where  $l$ =rupture length  
 332 (50 km),  $w$ =rupture width (30 km), and  $d$ =displacement (3.5 m) (Hanks and Kanamori, 1979,  
 333 adapted for dyne-cm):

$$M_w = \frac{2}{3} \log(3 \times 10^{11} \times l \times w \times d \times 10^{12} + 1) - 10.73$$

334 The result is an estimated  $M_w$  7.4, much higher than the past estimate of  $M$ 6.9 from intensity data  
 335 for the 1902 Shamakhi earthquake.

336 The lack of reported historical earthquakes farther to the west in the Kura fold-thrust belt  
 337 (i.e., near Goychay and west) contrasts with the numerous earthquakes reported near Shamakhi  
 338 over the past 4 centuries. Like prior authors, we expect that most large (e.g.  $M_w > 7$ ) earthquakes

339 would have been felt over a wide area and likely would have been recorded (Jackson and  
340 Ambraseys, 1997). Thus, the western and central Kura fold-thrust belt could either (a) have  
341 considerable strain accumulated or (b) be deforming aseismically. Given the numerous fault  
342 scarps identified during fieldwork (**Figure 2**) we suggest that the fault system does periodically  
343 produce surface rupturing earthquakes. If we assume that strain has accumulated at a rate of  $\sim 10$   
344 mm/yr since the earliest reported earthquake in AD 1139, then it is possible that 250 km of the  
345 Kura fold-thrust belt, from Agsu to Tbilisi, could have  $>8.8$  m of stored strain. The Kura fold-  
346 thrust belt soles into a  $5^\circ$  north-dipping detachment at a depth of  $\sim 5$  km (Forte et al., 2013), and  
347 the minimum width of the thrust belt is  $\sim 25$  km. The base of the seismogenic zone extends to at  
348 least a depth of 40 km in this region (Gunnels et al., 2021; Yetirmishli et al., 2021). Based on this  
349 geometry (width,  $w=25$  km, length,  $l=250$  km, displacement,  $d=8.8$ ), we can estimate a  
350 magnitude, were the whole fault to rupture, using the above equation. The result demonstrates  
351 that the Kura fold-thrust belt could have sufficient stored strain to produce a  $M_w > 8$  earthquake.  
352 This represents a significant hazard to the populations and infrastructure of the region, including  
353 the large earthen dam and  $15,730 \text{ km}^3$  reservoir at Mingecevir (**Figure 1**).

354 This contrast in earthquake histories between the main Kura fold-thrust belt and the  
355 eastern region near Shamakhi suggests that ruptures to the west are less frequent but could be  
356 significantly larger, while the Shamakhi region is affected by more frequent moderate ruptures.  
357 More paleoseismic trenching and detailed mapping will be required to confirm our results,  
358 ascertain the size of past ruptures in the Kura fold-thrust belt and to investigate how these  
359 ruptures are partitioned among the different thrust sheets.

## 360 **5 Conclusions**

361 The two surface rupturing events (AD 1713-1895 and AD 1872-2003) from the trench  
362 near Agsu are likely the surface ruptures of the historical 1668 and 1902 earthquakes that  
363 destroyed Shamakhi. We reassess the estimated magnitude for the 1902 event and suggest that it  
364 was a  $M_w 7.4$  rather than  $M 6.9$  earthquake. Further trenching is required to confirm these results,  
365 to place limits on the possible rupture lengths, to better estimate the magnitude of these historical  
366 events, and to determine the rupture histories of the other faults in the Kura fold-thrust belt to the  
367 west. Dating of an abandoned strath terrace in a water gap provides a maximum limit of  $\sim 8$   
368 mm/yr of shortening during the Holocene across the youngest active folds west of Agsu. These  
369 results are consistent with geodetic and structural studies that show that most of the  $\sim 10$  mm/yr  
370 of convergence between the Arabian plate and Eurasia in the western Greater Caucasus is  
371 accommodated by the Kura fold-thrust belt. Based on these rates, and if there have been no  
372 ruptures of the central and western parts of the Kura fold-thrust system since the last reported  
373 historical event in 1139 AD, then the system could have sufficient strain accumulated to produce  
374 a  $M > 8$  earthquake.

## 375 **Acknowledgements**

376 This research was supported in part by the Leverhulme Trust projects ‘EROICA’ (RPG-  
377 2018-371) and ‘NEPTUNE’ (RPG-2018-243), by the NERC-ESRC Increasing Resilience to  
378 Natural Hazards program ‘Earthquakes without Frontiers’ (NE/J02001X/1), the NERC-funded  
379 COMET (GA/13/M/031) and allocation 0009090 from the Research England GCRF support  
380 fund. The authors are grateful for field assistance from Sarvat Gurbanzada, Rashid Khalilov,  
381 Aslan Sadikov, Telman Jaferov, and Samandar Mammadov. Thanks to Arzu Javadova (SOCAR)

382 and Nazim Abdullayev (BP) for both their scientific input and for helping to organize funding  
383 from BP for field and laboratory expenses.

#### 384 **Data Availability Statement**

385 Drone photogrammetry models produced during this study are freely available on  
386 OpenTopography.org: <https://doi.org/10.5069/G93776XH>  
387 All other data used is publicly available or provided in this manuscript.

#### 388 **Conflict of Interest Statement**

389 The authors have no relevant financial or non-financial interests to disclose.

#### 390 **References**

- 391 Avdeev, B., Niemi, N.A., 2011. Rapid Pliocene exhumation of the central Greater Caucasus  
392 constrained by low-temperature thermochronometry. *Tectonics* 30.  
393 <https://doi.org/10.1029/2010TC002808>
- 394 Bronk Ramsey, C., 1995. Radiocarbon Calibration and Analysis of Stratigraphy: The OxCal  
395 Program. *Radiocarbon* 37, 425–430. <https://doi.org/10.1017/S0033822200030903>
- 396 Cowgill, E., Forte, A.M., Niemi, N., Avdeev, B., Tye, A., Trexler, C., Javakhishvili, Z.,  
397 Elashvili, M., Godoladze, T., 2016. Relict basin closure and crustal shortening budgets  
398 during continental collision: An example from Caucasus sediment provenance. *Tectonics*  
399 35, 2918–2947. <https://doi.org/10.1002/2016TC004295>
- 400 Forte, A.M., Cowgill, E., Murtuzayev, I., Kangarli, T., Stoica, M., 2013. Structural geometries  
401 and magnitude of shortening in the eastern Kura fold-thrust belt, Azerbaijan: Implications  
402 for the development of the Greater Caucasus Mountains. *Tectonics* 32, 688–717.  
403 <https://doi.org/10.1002/tect.20032>
- 404 Forte, A.M., Sumner, D.Y., Cowgill, E., Stoica, M., Murtuzayev, I., Kangarli, T., Elashvili, M.,  
405 Godoladze, T., Javakhishvili, Z., 2015. Late Miocene to Pliocene stratigraphy of the Kura  
406 Basin, a subbasin of the South Caspian Basin: implications for the diachroneity of stage  
407 boundaries. *Basin Res.* 27, 247–271. <https://doi.org/10.1111/bre.12069>
- 408 Gunnels, M., Yetrimishli, G., Kazimova, S., Sandvol, E., 2021. Seismotectonic evidence for  
409 subduction beneath the Eastern Greater Caucasus. *Geophys. J. Int.* 224, 1825–1834.  
410 <https://doi.org/10.1093/gji/ggaa522>
- 411 Hanks, T.C., Kanamori, H., 1979. A moment magnitude scale. *J. Geophys. Res. Solid Earth* 84,  
412 2348–2350. <https://doi.org/10.1029/JB084iB05p02348>
- 413 Ismail-Zadeh, A., Adamia, S., Chabukiani, A., Chelidze, T., Cloetingh, S., Floyd, M., Gorshkov,  
414 A., Gvishiani, A., Ismail-Zadeh, T., Kaban, M.K., Kadirov, F., Karapetyan, J., Kangarli,  
415 T., Kiria, J., Koulakov, I., Mosar, J., Mumladze, T., Müller, B., Sadradze, N., Safarov, R.,  
416 Schilling, F., Soloviev, A., 2020. Geodynamics, seismicity, and seismic hazards of the  
417 Caucasus. *Earth-Sci. Rev.* 207, 103222. <https://doi.org/10.1016/j.earscirev.2020.103222>
- 418 Jackson, J., Priestley, K., Allen, M., Berberian, M., 2002. Active tectonics of the South Caspian  
419 Basin. *Geophys. J. Int.* 148, 214–245. <https://doi.org/10.1046/j.1365-246X.2002.01588.x>

- 420 Jackson, J.A., Ambraseys, N.N., 1997. Convergence between Eurasia and Arabia in eastern  
421 Turkey and the Caucasus, in: *Historical and Prehistorical Earthquakes in the Caucasus*, 28.  
422 pp. 79–90.
- 423 Kadirov, F., Floyd, M., Alizadeh, A., Guliev, I., Reilinger, R., Kuleli, S., King, R., Nafi Toksoz,  
424 M., 2012. Kinematics of the eastern Caucasus near Baku, Azerbaijan. *Nat. Hazards* 63,  
425 997–1006. <https://doi.org/10.1007/s11069-012-0199-0>
- 426 Kangarli, T.N., Kadirov, F.A., Etirmishli, G.D., Aliev, F.A., Kazimova, S.E., Aliev, A.M.,  
427 Safarov, R.T., Vakhabov, U.G., 2018. Geodynamics, active faults and earthquake source  
428 mechanisms in the zone of pseudosubduction interaction of continental microplates in the  
429 South and North Caucasus (southern slope of the Greater Caucasus, Azerbaijan). *Geodyn.*  
430 *Tectonophys.* 9, 1099–1126. <https://doi.org/10.5800/GT-2018-9-4-0385>
- 431 Le Brun, C., 1759. *A New and More Correct Translation than Has Hitherto Appeared in Public*  
432 *of Mr. Cornelius Le Brun's Travels into Moscovy, Persia, and Divers Parts of the East-*  
433 *Indies; Containing An Accurate Description of All Such Articles as Are Most Remarkable*  
434 *in Each of Those Different Countries, and Most Worthy the Attention of the Curious*  
435 *Reader. As Also Of Their Antiquities; but More Particularly Those Relating to the Famous*  
436 *Palace of Persepolis, Commonly Called Chelminar by the Persians: By a Gentleman of*  
437 *Oxford. J. Warcus, London.*
- 438 McCalpin, J. (Ed.), 2009. *Paleoseismology*, 2nd ed. ed, International geophysics series.  
439 Academic Press, Burlington, MA.
- 440 McKenzie, D., 1972. Active Tectonics of the Mediterranean Region. *Geophys. J. Int.* 30, 109–  
441 185. <https://doi.org/10.1111/j.1365-246X.1972.tb02351.x>
- 442 Mosar, J., Kangarli, T., Bochud, M., Glasmacher, U.A., Rast, A., Brunet, M.-F., Sosson, M.,  
443 2010. Cenozoic-Recent tectonics and uplift in the Greater Caucasus: a perspective from  
444 Azerbaijan. *Geol. Soc. Lond. Spec. Publ.* 340, 261–280. <https://doi.org/10.1144/SP340.12>
- 445 Mumladze, T., Forte, A.M., Cowgill, E.S., Trexler, C.C., Niemi, N.A., Burak Yikilmaz, M.,  
446 Kellogg, L.H., 2015. Subducted, detached, and torn slabs beneath the Greater Caucasus.  
447 *GeoResJ* 5, 36–46. <https://doi.org/10.1016/j.grj.2014.09.004>
- 448 New York Times, T., 1902. 2,000 DEAD AT SHEMAKHA. *N. Y. Times* 1.
- 449 Nikonov, A.A., 1982. Sil'neishee Zemletriasenie Bol'shogo Kavkaza 14 Ianvaria 1668 g. *Fis.*  
450 *Zemli* 9, 90–106.
- 451 Philip, H., Cisternas, A., Gvishiani, A., Gorshkov, A., 1989. The Caucasus: an actual example of  
452 the initial stages of continental collision. *Tectonophysics* 161, 1–21.  
453 [https://doi.org/10.1016/0040-1951\(89\)90297-7](https://doi.org/10.1016/0040-1951(89)90297-7)
- 454 Pigati, J.S., Rech, J.A., Nekola, J.C., 2010. Radiocarbon dating of small terrestrial gastropod  
455 shells in North America. *Quat. Geochronol.* 5, 519–532.  
456 <https://doi.org/10.1016/j.quageo.2010.01.001>
- 457 Reilinger, R., McClusky, S., Vernant, P., Lawrence, S., Ergintav, S., Cakmak, R., Ozener, H.,  
458 Kadirov, F., Guliev, I., Stepanyan, R., Nadariya, M., Hahubia, G., Mahmoud, S., Sakr, K.,  
459 ArRajehi, A., Paradissis, D., Al-Aydrus, A., Prilepin, M., Guseva, T., Evren, E., Dmitrotsa,

- 460 A., Filikov, S.V., Gomez, F., Al-Ghazzi, R., Karam, G., 2006. GPS constraints on  
461 continental deformation in the Africa-Arabia-Eurasia continental collision zone and  
462 implications for the dynamics of plate interactions. *J. Geophys. Res. Solid Earth* 111.  
463 <https://doi.org/10.1029/2005JB004051>
- 464 Shebalin, N.V., Kondorskaia, N.V., World Data Center A for Solid Earth Geophysics, 1982.  
465 New catalog of strong earthquakes in the U.S.S.R. from ancient times through 1977,  
466 Report SE ;31. World Data Center A for Solid Earth Geophysics, Boulder, Colo.
- 467 Tavernier, J.-B., 1678. *The Six Voyages of John Baptista Tavernier, a Noble Man of France*  
468 *Now Living, through Turkey into Persia and the East-Indies, Finished in the Year 1670 :*  
469 *Giving an Account of the State of Those Countries : Illustrated with Divers Sculptures ;*  
470 *Together with a New Relation of the Present Grand Seignor's Seraglio, by the Same*  
471 *Author.* John Philips, London.
- 472 Telesca, L., Kadirov, F., Yetirmishli, G., Safarov, R., Kazimova, S., 2018. Joint Use of  
473 Seismological and Topological Statistical Methods for the Analysis of 2010–2016  
474 Azerbaijan Seismicity. *Pure Appl. Geophys.* 175, 4225–4239.  
475 <https://doi.org/10.1007/s00024-018-1945-3>
- 476 Weber, V., 1903. Shamakhi Earthquake of 13 February 1902, Proceedings of the St. Petersburg  
477 Geological Committee.
- 478 Yetirmishli, G.J., Ismayilova, S.S., Kazimova, S.E., 2021. Seismicity of the territory of  
479 Azerbaijan in 2019. *Seism. Obs. Territ. Azerbaijan* 19, 3–18.
- 480 Yetirmishli, G.J., Kazimov, I.E., Kazimova, A.F., 2022. Analysis of Modern Movements of  
481 Earth Crust Blocks in Azerbaijan According to the Data of GPS Stations in 2020-2021.  
482 *Seism. Obs. Territ. Azerbaijan* 21, 19–24.
- 483 Zhang, H., Aldana-Jague, E., Clapuyt, F., Wilken, F., Vanacker, V., Van Oost, K., 2019.  
484 Evaluating the potential of post-processing kinematic (PPK) georeferencing for UAV-  
485 based structure- from-motion (SfM) photogrammetry and surface change detection. *Earth*  
486 *Surf. Dyn.* 7, 807–827. <https://doi.org/10.5194/esurf-7-807-2019>
- 487

488 **Table 1. Radiocarbon sample data**

Sample Name	Location	Unit	Lat. (°)	Lon. (°)	Sample Material <sup>1</sup>	Radiocarbon Age (BP)	Calibrated <sup>2</sup> Age (AD)	OxCal <sup>2</sup> v4.4 Modeled Age (AD, 95.4%)	Percent Modern Carbon (pMC)	δ13C (‰)	δ18O (‰)
R1	Agsu T1	U4	40.572	48.427	Charcoal	-20 ± 30	1954-1957 (60.9%) 1886-1913 (31.0%) 1707-1718 (2.4%) 1825-1832 (1.2%)	1811-1917	100.25 ± 0.37	-27.0	-
R5	Agsu T1	U4	40.572	48.427	Plant material	-2080 ± 30	1978-1979 (89.3%) 1961 (6.1%)	-	129.55 ± 0.48	-24.8	-
R6	Agsu T1	U4	40.572	48.427	Charcoal	190 ± 30	1724-1812 (52.0%) 1648-1695 (21.8%) 1916- >1950(17.8%) 1838-1878 (3.8%)	1739-1948	97.66 ± 0.36	-24.9	-
R7	Agsu T1	U5	40.572	48.427	Plant material	-770 ± 30	1996-2000 (92.9%) 1956-1957 (2.5%)	-	110.06 ± 0.41	-28.0	-
R10	Agsu T1	U2	40.572	48.427	Plant Material	-3410 ± 30	1967-1971 (93.2%) 1962 (2.2%)	-	152.88 ± 0.57	-25.8	-
R11	Agsu T1	U2	40.572	48.427	Plant Material	1240 ± 30	758-880 (55.8%) 679-746 (39.6%)	695-887	85.7 ± 0.32	-26.3	-
R18	Agsu T1	U5	40.572	48.427	Plastic candy wrapper	-	-	1985-2006	-	-	-
R24	Agsu T1	U2	40.572	48.427	Charcoal	70 ± 30	1810-1919 (68.7%) 1692-1727 (26.7%)	1683-1853	99.13 ± 0.37	-23.5	-
R25	Agsu T1	U2	40.572	48.427	Organic Sediment*	1160 ± 30	820-978 (83.9%) 772-790 (10.2%) 804-810 (1.3%)	774-979	86.55 ± 0.32	-	-
R26	Agsu T1	U1	40.572	48.427	Organic Sediment*	940 ± 30	1028-1172 (95.4%)	1028-1171	88.96 ± 0.33	-26.2	-
R29	Agsu T1	U1	40.572	48.427	Charcoal	120 ± 30	1799-1940 (67.2%) 1680-1740 (25.8%) 1752-1764 (2.4%)	1669-1859	98.52 ± 0.37	-26.3	-
R31	Agsu T1	U3	40.572	48.427	Charcoal	690 ± 30	1272-1317 (65.5%) 1360-1388 (29.9%)	1271-1389	91.77 ± 0.34	-25.4	-
R33	Agsu T1	W2	40.572	48.427	Plant Material	-150 ± 30	1954-1956 (95.4%)	-	101.88 ± 0.38	-29.0	-
R35	Agsu T1	W2	40.572	48.427	Charcoal	160 ± 30	1719-1786 (31.6%) 1906->1950(19.4%) 1832-1892 (17.9%) 1664-1708 (16.7%) 1792-1819 (9.8%)	1741-1948	98.03 ± 0.37	-25.6	-
R37	Agsu T1	U2	40.572	48.427	Charcoal	180 ± 30	1722-1814 (49.9%) 1656-1698 (19.2%) 1910->1950(19.0%) 1836-1880 (7.3%)	1650-1810	97.78 ± 0.37	-23.6	-
WG1	Water gap	-	40.559	48.236	Shell <sup>†</sup>	6040 ± 30	5026-4842 BC (95.4%)	-	47.15 ± 0.18	-7.8	-2.23

<sup>1</sup>All samples pretreated with acid/alkali/acid washes unless otherwise noted.

\*Acid wash pretreatment only

†Acid etch pretreatment only

<sup>2</sup>All calibrations were done with OxCal v4.4 using the IntCal 20 curve.